Nucleation and Isothermal Crystallization of the Polyethylene Block within Diblock Copolymers Containing Polystyrene and Poly(ethylene-*alt*-propylene)

A. T. Lorenzo,[†] M. L. Arnal,[†] A. J. Müller,*[,†] A. Boschetti-de-Fierro,[‡] and V. Abetz[‡]

Grupo de Polímeros USB, Departamento de Ciencia de los Materiales, Universidad Simón Bolívar, Apartado 89000, Caracas 1080-A, Venezuela, and Institut für Polymerforschung, GKSS-Forschungszentrum Geesthacht GmbH, 21502 Geesthacht, Germany

Received January 29, 2007; Revised Manuscript Received May 3, 2007

ABSTRACT: The crystallization kinetics of the polyethylene block within polyethylene-*b*-polystyrene (PE-*b*-PS) and polyethylene-*b*-poly(ethylene-*alt*-propylene) (PE-*b*-PEP) diblock copolymers has been investigated in a wide composition range by differential scanning calorimetry (DSC) and compared to an equivalent homopolymer. The morphology of the copolymers in the melt and its changes after crystallization were explored by small-angle X-ray scattering (SAXS) experiments. SAXS experiments demonstrated that PE-*b*-PS formed microdomain ordered structures in the melt. On the basis of the lamellar morphology that was developed by PE-*b*-PEP (demonstrated by transmission electron microscopy, TEM) regardless of composition, it was deduced that these diblocks crystallize from either a homogeneous or a weakly segregated melt. Also, the effects of the neighboring block on thermal fractionation of the PE block were obtained by successive self-nucleation and annealing (SSA). Classical kinetics theories of polymer nucleation and crystallization were applied to DSC overall isothermal crystallization data. The energetic parameters obtained allow us to quantitatively estimate the increase in the energy barrier for crystallization of the PE block, caused by the covalently bonded PEP and PS block as compared to homo-PE. Also, the Lauritzen and Hoffman theory was applied to DSC isothermal crystallization of previously self-nucleated PE (where crystal growth is the dominant factor), and the contributions of nucleation and growth were estimated. Using this novel approach, we demonstrate that the nucleation process is the rate-determining step in the crystallization behavior of highly confined PE-*b*-PS diblock copolymers, results that were corroborated by the low Avrami index values found in these diblock copolymers. Similar trends were obtained by applying polymer nucleation theories. In the case of PE-*b*-PEP diblock copolymers, the energy barrier associated with nucleation and growth increases as the PEP content within the copolymers increases. The PEP block acts as a diluent for the PE block crystallization in view of the miscibility between the blocks.

Introduction

Block copolymers have received considerable attention, both theoretically and experimentally, due to their ability to self-organize in a great variety of fascinating morphologies on the scale of micro- and nanometers (commonly referred to as microdomains, MDs). In addition, block copolymers offer the opportunity to control the size and morphology of the MDs by changing one or more of the following parameters: molecular weight, molecular architecture, molecular structure, segregation strength, composition, and sample preparation.[1] Many of the interesting properties that these material exhibit can be attributed to their tendency to separate into microphases.[2−5]

In the case of block copolymers with one or more crystallizable blocks, the phase separation can be more complex.[6−8] The crystallization process could disrupt the original morphology presented in the molten state, and it can be the driving force to the formation of the final solid-state morphology. At the same time, the presence of the amorphous block could affect the crystallization behavior.[5,6] It is generally accepted that, besides the segregation strength and the composition, the changes of state as a function of temperature can determine the final morphology according to three transition temperatures: the order−disorder transition temperature (T_{ODT}), the glass transition (T_g) of the amorphous block, and the crystallization temperature (T_c) of the crystallizable one.[7] The most common cases presented in the literature will be briefly discussed below.

Homogeneous Melt ($T_{ODT} < T_c > T_g$). In diblock copolymers with a homogeneous melt, the microphase separation is driven by the crystallization process if the T_g of the amorphous block is lower than the T_c of the crystallizable block. This case generally results in a lamellar morphology where crystalline lamellae are sandwiched by the amorphous block layers. This behavior has been observed in various systems, for example, in the diblock copolymer of ethylene-*b*-(3-methyl-1-butene) (EMB),[9,10] where even for very low polyethylene contents (i.e., f_E: 0.12) the final morphology after the crystallization of the PE block was that of lamellae. In another work, Bodganov et al.[11] reported results on the crystallization of diblock copolymers of poly(ϵ-caprolactone)-*b*-poly(ethylene glycol) (EGC; f_{EG}: 0.20) and established that the crystallization of one or both crystallizable blocks will depend upon the cooling conditions employed. From a homogeneous melt, when the diblock copolymer is cooled to a temperature above the melting point of the PEG ($T_c = 30-42$ °C), only the PCL block crystallized at a global rate very similar to that observed for the PCL homopolymer (of similar molecular weight). If a lower range of T_c was employed ($T_c = 15-25$ °C), the diblock copolymer formed a lamellar morphology after the crystallization process of both blocks occurred.

Rangarajan et al.[12−14] studied the dynamics of the crystallization-driven microphase separation of polyethylene-*b*-poly(ethylene-*alt*-propylene) (E/EP) diblock copolymers. They

* To whom correspondence should be addressed. E-mail: amuller@usb.ve.
[†] Universidad Simón Bolívar.
[‡] GKSS-Forschungszentrum Geesthacht GmbH.

10.1021/ma070252l CCC: $37.00
Published on Web 06/13/2007

Table 1. Characteristics of the Samples Employed

copolymers	wt_{PE}[a]	ϕ_{PE}[b]	M_n (kg/mol) PE block[c]	PE % 1,2 units[d]	PEP % 1,4 units[d]	PEP % 1,2 and 3,4 units[d]	polydisp D[c]
PE^{25}			25	11.0			1.01
$E_{53}S_{47}{}^{51}$	0.53	0.57	27	11.3			1.04
$E_{26}S_{74}{}^{105}$	0.26	0.29	27	11.3			1.05
$E_{11}S_{89}{}^{244}$	0.11	0.13	27	11.3			1.02
$E_{54}EP_{46}{}^{53}$	0.54	0.52	29	11.2	88.7	11.3	1.02
$E_{29}EP_{71}{}^{99}$	0.29	0.28	29	11.9	86.4	13.6	1.02
$E_{12}EP_{88}{}^{238}$	0.12	0.11	28	11.2	88.8	11.2	1.03

[a] Weight fraction of the PE block. [b] PE block volumetric fraction determined assuming additive volumes. Densities at room temperature of the PE semicrystalline block were employed using the corresponding crystallinity degrees calculated by DSC, and crystalline and amorphous values taken from the literature ($\rho_{PS} = 1.05$ g/cm^3; $\rho_{am-PE} = 0.887$ g/cm^3; $\rho_{cr-PE} = 0.999$ g/cm^3; $\rho_{PEP} = 0.854$ g/cm^3).[22] [c] Determined by SEC experiments. [d] Determined by ^{1}H NMR experiments.

established that the crystallization of the ethylene block exactly tracks the development of the microdomain structure; from SAXS/WAXS (small-angle X-ray scattering/wide-angle X-ray scattering) results they concluded that during the initial rapid structure development, at the crystallization temperature, the SAXS peaks positions are constant, suggesting that the ordered structures nucleate and simply grow until they fill the crystallizable sample as observed, commonly, in homopolymers.

Okamoto et al.[15] evaluated the crystallization of a PE-*b*-PEP diblock copolymer with a 0.52 weight fraction of PE. By differential scanning calorimetry (DSC), SAXS, and WAXS experiments they found that the structure and morphology in this diblock copolymer are dominated by the PE crystallization from a disordered state. They found, by dynamic mechanical experiments, that the T_{ODT} value was below (105 ± 5 °C) the melting point of this sample (108 °C), confirming that the melt was homogeneous.

Soft Confinement and Break-Out Cases ($T_{ODT} > T_c > T_g$). The final morphology will depend on the segregation strength χN of the system (where χ is the Flory−Huggins interaction parameter and N is the block copolymer total chain length).[4−6] First, for systems within the weak segregation limit (WSL or low χN) the crystallization process will be the driving force for the solid-state final morphology, and the crystallization will provoke a "break-out" of the melt morphology originating an interconnected morphology. Second, if the copolymers are within the intermediate segregation limit (ISL or medium χN), the thermal treatment employed for the crystallization will determine the final microphase morphology obtained: (i) if a quenching from the melt is employed, the melt morphology will be retained after the crystallization process; (ii) in contrast, if a controlled cooling from the melt is used (isothermal crystallization or slow cooling rates), the melt morphology is disrupted (break-out crystallization) and the solid-state morphology is driven by the crystallization. Third, for block copolymers within the strong segregation limit (SSL or high χN), the crystallization process is not able to break out or disrupt the melt morphology.

Quiram et al.[9,10] studied weakly segregated diblock copolymers of polyethylene-*b*-poly(3-methyl-1-butene) (EMB), with crystallization resulting in a morphology which is strongly dependent on thermal history. Fast cooling kinetically confines crystallization to cylinders, and a spherulitic superstructure is not formed. Slow cooling allows crystallization to break out the preestablished melt mesophase, and the copolymer forms a lamellar morphology exhibiting a larger Bragg spacing than the melt, with the additional development of a spherulitic superstructure. Similar results were found by Rangarajan et al.[16] using polyethylene-*b*-poly(hh-propylene) (EhhP) and Nojima et al.[17] in their work with polybutadiene-*b*-poly(ϵ-caprolactone) (BCl).

Hard Confinement ($T_{ODT} > T_g > T_c$). For strongly segregated block copolymers where the T_g of the amorphous block is above the T_c of the crystallizable block, the melt morphology is kept after the crystallization process takes place.[18−21] For the copolymer having a glassy amorphous component, it is expected that the crystallizable segments are forced to crystallize within a limited space (MDs) like spheres, cylinders, and lamellae. Therefore, there is a direct relationship between the morphology (MDs) and the crystallization kinetics.

In this paper we will present the comparison of the nucleation and crystallization kinetics of the polyethylene block covalently bonded to a glassy block (polystyrene) or to a rubbery block (poly(ethylene-*alt*-propylene)). The PE-*b*-PS block copolymers are strongly segregated in the melt, and the crystallization of the PE block will also occur under hard confinement conditions (because of the glassy PS matrix at the PE block crystallization temperatures); therefore, a morphology of well-segregated MDs (spheres, cylinders, and lamellae) is expected. In contrast, the PE-*b*-PEP diblock copolymers form a homogeneous or weakly segregated melt, the PEP block is rubbery at the PE crystallization temperatures, and the crystallization will be strongly affected by the diluent effect of the PEP block upon the PE block. A lamellar morphology is expected regardless of composition for the PE-*b*-PEP case since PE crystallization will drive structure formation.

Experimental Section

Synthesis. The synthesis of poly(1,4-butadiene)-*b*-polystyrene diblock copolymers (PB-*b*-PS), poly(1,4-butadiene)-*b*-poly(1,4-isoprene) diblock copolymers (PB-*b*-PI), and poly(1,4-butadiene) (PB) homopolymer was accomplished by sequential anionic polymerization of butadiene, styrene, and isoprene, in benzene at 40 °C (for styrene) and 60 °C (for butadiene and isoprene) with *sec*-BuLi as initiator. The use of benzene as a solvent results in a high 1,4-addition for butadiene and isoprene, which particularly for butadiene is indispensable to get a "pseudo-polyethylene" structure after hydrogenation.[20] The reaction was terminated using isopropanol followed by precipitation in the same solvent. SEC experiments of the PB homopolymer and the non-hydrogenated diblock copolymer solutions in THF (2% w/v) were performed on a Waters instrument calibrated with narrowly distributed polybutadiene standards at 30 °C and with a flow rate of 1 mL/min using toluene as internal standard. In the notation $A_xB_y{}^m$ here employed, the subscript numbers denote the mass fraction in weight percent and the superscript gives the number-averaged molecular weight M_n in kg/mol of the entire block copolymer (see Table 1). The copolymer compositions and molecular weight were obtained using ^{1}H NMR spectroscopy (Bruker AC 250 spectrometer) in $CDCl_3$. Also, the % (1,2) units for the polybutadiene and % (1,2), (1,4), and (3,4) units for the polyisoprene block were calculated using ^{1}H NMR. More details can be found elsewhere.[20]

The synthesis procedure employed here was designed to obtain a PE block within the block copolymers with similar molecular weight and the same content of 1,2 units as in the PE homopolymer (see Table 1). In this way, we have eliminated the influence of

these parameters in the thermal and morphological behavior of the diblock copolymers, allowing us to make more meaningful comparisons between the diblock copolymer system and the PE homopolymer.

Hydrogenation. The polyethylene-*b*-polystyrene diblock copolymers (PE-*b*-PS), polyethylene-*b*-poly(ethylene-*alt*-propylene) (PE-*b*-PEP), and PE homopolymer (PE) were obtained by hydrogenation of the corresponding precursors PB-*b*-PS, PB-*b*-PI, and PB. Homogeneous catalytic hydrogenation was carried out in degassed toluene (1.5−2 wt % solution of the polymer) at 60 °C and 60 bar H_2 pressure for 3 days using a Wilkinson catalyst $(Ph_3P)_3Rh(I)Cl$ (Aldrich, 1 mol % with respect to the number of double bonds present in the PB and PI block). Under the employed conditions the PB and PI blocks get completely hydrogenated as revealed by ^1H NMR (results not shown). Purification was accomplished by precipitation into isopropanol. Further purification was performed in order to remove residual the Wilkinson catalyst by refluxing the homopolymer or block copolymer solution in toluene with a small amount of concentrated hydrochloric acid, again followed by precipitation into isopropanol.

Differential Scanning Calorimetry (DSC). Samples of approximately 5−7 mg were encapsulated in aluminum pans and measured in a Perkin-Elmer Pyris 1 calibrated with naphthalene and indium under a high-purity nitrogen atmosphere. The thermal protocols employed are described next.

Standard DSC Experiments. In the standard DSC dynamic experiments the DSC scans were obtained at 10 °C/min. All DSC cooling curves were recorded after the samples were held in the melt at 140 °C for 3 min in order to erase all previous crystalline history of the PE block. The crystallization and melting enthalpies values were normalized with respect to the PE fraction within the block copolymers.

Isothermal DSC Experiments. In the isothermal crystallization experiments the samples were held in the melt at 140 °C for 3 min in order to erase all previous crystalline history of PE and then quickly cooled (at 80 °C/min) to the desired crystallization temperature (T_c) where the isothermal DSC scan was recorded. Experiments were performed to ensure that the samples did not crystallize during cooling to T_c by immediately heating the samples when the temperature reached the desired T_c; if any melting occurred, then it was concluded that the crystallization took place during cooling and the isothermal experiment was not performed at that T_c. This procedure was repeated until no crystallization during cooling was evident.

When the PE content was low in the block copolymer (below 30%), the conventional isothermal kinetics were beyond the resolution of the DSC (i.e., the amount of heat evolved per unit time was too small to be measured isothermally). The isothermal crystallization was instead performed by a step procedure described as follows: (a) erasure of crystalline history by heating the sample to 140 °C and holding it at that temperature for 3 min; (b) fast cooling (80 °C/min) down to T_c; (c) the sample was held at T_c for a time t_c, which was later increased in the subsequent steps; (d) heating at 10 °C/min from T_c to 140 °C. The heat of fusion calculated from this DSC heating scan should correspond to the crystallization enthalpy of the crystals formed during step ''c" at T_c for the specified crystallization time; (e) steps a−d were repeated employing the same T_c in step ''b", but at increasing t_c. The last t_c was taken as the time the melting enthalpy in the subsequent heating scan did not change with respect to the previous one; (f) the whole process was repeated for different T_c temperatures.

Self-Nucleation Experiments (SN). The self-nucleation and annealing experiment using DSC was originally applied by Fillon et al.[23] to isotactic polypropylene (PP). These experiments involved the partial melting of a crystalline "standard" state followed by recrystallization using as nuclei the crystal fragments produced in the partial melting stage. The detailed procedure used here is described as follows: (a) Erasure of any previous crystalline history by heating the sample up to 140 °C for 3 min. (b) Creation of a "standard" crystalline history by cooling at a rate of 10 °C/min to 0 °C. This step ensures that the crystallization of the polymer under investigation occurs at the same dynamic conditions. (c) Heating at 10 °C/min up to a self-nucleation temperature (T_s). (d) The thermal conditioning at T_s is performed for 5 min. (e) DSC cooling scans from T_s until 0 °C at a rate of 10 °C/min, where the effects of the thermal treatment will be reflected on the crystallization of PE. (f) DSC heating scans from 0 to 140 °C, where the effects of the entire thermal treatment will also be reflected in the melting of PE. Depending on T_s, selected for step d and according to Fillon et al.,[23] the sample will be completely molten, self-nucleated, or self-nucleated and annealed. If T_s is too high, no self-nuclei or crystal fragments can survive, and the sample is said to be in domain I or complete melting domain. When T_s is high enough to melt the sample almost completely, but low enough to leave active self-nuclei (Fillon et al.[23] propose that the self-nuclei are crystal fragments; however, more recently it has been proposed that such self-nuclei could be composed of crystallization precursors or by molecules that retain crystalline memory of the material, i.e., local segmental orientation[24]), the crystallization peak shifted to higher temperatures during the subsequent cooling from T_s; the sample is said to be in domain II or self-nucleation domain. When T_s is too low, only part of the crystals will melt. Therefore, the unmolten crystals will be annealed during the 5 min at T_s, while the rest of the polymer will be self-nucleated during the subsequent cooling from T_s; then the sample is said to be in domain III or self-nucleation and annealing domain. Isothermal crystallization of some chains during the 5 min at T_s can also occur when T_s is within domain III. The domains can be distinguished by careful observations of the cooling runs (step e) from T_s and the final heating runs (step f). For instance, if annealing took place at T_s, then a second, higher melting peak might be seen.

Successive Self-Nucleation and Annealing Experiments (SSA). The SSA technique was developed by Müller et al.[25,26] and enhances the potential molecular fractionation that occurs during crystallization, while encouraging annealing of the unmolten crystals at each stage of the process, so that small effects can be magnified.

Experimentally, steps a−d of the SN method described above were repeated as the first part of this experiment. Special care should be taken in choosing the first T_s temperature to be used in step d. Ideally, the first T_s should be high enough to melt most of the polymer but low enough to leave active self-nuclei at that T_s. The following steps were performed immediately after steps a−d:

(e) Cooling from T_s: The sample was cooled at 10 °C/min from T_s to 0 °C. During this process, the initially molten fraction of the polymer at T_s will crystallize during cooling using the unmolten crystal fragments produced in step c as self-nuclei.

(f) Heating up to a new T_s: The sample was heated once again at 10 °C/min, but this time up to a T_s which was 5 °C lower than the previous one, and this temperature was held for 5 min. This means that the unmolten crystallites at this T_s will anneal and some of the molten species may isothermally crystallize (after being self-nucleated by the unmolten crystals) while the rest of the molten crystallizable chain segments will only crystallize during the subsequent cooling from T_s.

Steps e and f are repeated at increasingly lower T_s. The differences in T_s were always kept constant at 5 °C. The number of repetitions can be chosen to cover the entire melting range of the sample with a "standard" crystalline history or a shorter range.

(g) Final melting: The sample was heated at 10 °C/min from 0 to 140 °C, and a multiple melting endotherm was obtained.

The SSA procedure was performed for the PE homopolymer, choosing a T_s of 102 °C as the ideal self-nucleation temperature, and the T_s temperatures were varied from 102 to 72 °C at 5 °C intervals for a total of seven self-nucleation/annealing steps. The same parameters were applied to all the diblock copolymer samples in order to maintain a standard thermal treatment based on the homopolymer.

Transmission Electron Microscopy (TEM). The bulk morphology of the PE-*b*-PS and PE-*b*-PEP diblock copolymers were examined by bright field TEM using a JEOL 1220 operated at 100 kV. Films around 1 mm thick were prepared by casting from a 3 wt % solution of the sample in toluene at 70 °C in order to avoid

Table 2. Polymerization Degree, *N*, of the Corresponding Block and the Segregation Strength (χN) Values Calculated at 25 and 150 °C

					χN[a]	
copolymers	N_{PE}	N_{PS}	N_{PEP}	N_{total}	25 °C	150 °C
$E_{53}S_{47}{}^{51}$	964	231		1195	115	81
$E_{26}S_{74}{}^{105}$	975	747		1722	165	116
$E_{11}S_{89}{}^{244}$	957	2088		3046	292	206
$E_{54}EP_{46}{}^{53}$	1022		348	1370	13	9
$E_{29}EP_{71}{}^{99}$	1025		1004	2030	19	13
$E_{12}EP_{88}{}^{238}$	932		2991	3924	36	26

[a] The Flory−Huggins enthalpic segmental interaction parameters, χ, were calculated using the following equations: (i) for PE-*b*-PS, $\chi_{E/S}(T) = 28.608/T$,[27] and (ii) for PE-*b*-PEP, $\chi_{E/PEP}(T) = 2.752/T$.[28]

gelation upon solvent evaporation. After complete evaporation of the solvent (ca. 1 week), the films were kept at 150 °C for 15 h in order to improve the morphological segregation; next, these samples were kept for 3 h at a specific crystallization temperature in order to allow for maximum crystallization of the PE block. Later, the films were slowly cooled to room temperature. Thin sections were cut at −130 °C using a LEICA EMFCS ultramicrotome equipped with a diamond knife. Staining of the hydrogenated diblock copolymers was accomplished by exposing thin sections to RuO_4 (preferential staining of the amorphous PS and PEP blocks).

Small-Angle X-ray Scattering (SAXS). Bulk morphology of diblock copolymers was determined by means of temperature-dependent small-angle X-ray scattering (SAXS) at the A2 beamline of DORIS, HASYLAB, DESY, using a sample−detector distance of 3040 mm and a wavelength of 1.5 Å. A temperature chamber was employed using liquid nitrogen as cooling fluid. The experiments shown here correspond to small-angle X-ray scattering recorded during a heating−cooling cycle. The samples were held for 1 min at the initial temperature of 25 °C, then heated up to 150 °C at 10 °C/min, held there for 3 min, and then cooled to 25 °C at 10 °C/min. The diffraction patterns were obtained with frames taken for 10 s every 15 s.

Results and Discussion

1. Morphology. In this publication we compare the crystallization behavior of two sets of PE containing diblock copolymers. In the first case, the PE-*b*-PEP diblock copolymers possess χN values between 13 and 36 (at 25 °C) which indicate a behavior in between total miscibility of both blocks and weak segregation strength (especially for $\chi N = 36$).[4−6] In the second case, the PE-*b*-PS system has χN values between 115 and 292 (at 25 °C), which are typical values for block copolymers within the strong segregation limit (SSL). In Table 2, the polymerization degree *N* of each block is presented along with the segregation strength χN for 25 and 150 °C, i.e., solid and molten state, respectively.

Figure 1 shows representative TEM micrographs of selected PE-*b*-PEP and PE-*b*-PS diblock copolymers. For the PE-*b*-PEP diblock copolymers, the micrographs presented in Figure 1 ($E_{54}EP_{46}{}^{53}$ and $E_{29}EP_{71}{}^{99}$) show the crystalline lamellae formed by the crystallizable fraction of the PE block within the amorphous matrix of the miscible amorphous PE and the PEP components. Unfortunately, because of the low content of PE in $E_{12}EP_{88}{}^{238}$, good quality TEM images were not obtained. The crystalline fraction found for PE crystallization within $E_{54}EP_{46}{}^{53}$ and $E_{29}EP_{71}{}^{99}$ was ∼27% in both cases. Similar results have been reported for weakly segregated systems like PE-*b*-PEP and PE-*b*-poly(ethylethylene) (PE-*b*-PEE), where the PEP and PEE blocks are rubbery at the crystallization temperatures of the PE block.[29] Therefore, on the basis of literature on similar copolymers and on the TEM images presented in Figure 1, we can conclude that crystallization drives structure formation and that the copolymers must be either weakly segregated or homogeneous in the melt state.

SAXS measurements were performed on the PE-*b*-PEP diblock copolymer samples and maxima related to lamellar periods were observed only in annealed or isothermally crystallized samples when the patterns were recorded at 25 °C. However, at 150 °C, the difference in electron densities is so small in between the two molten components that no correlation hole or any other signal was observed in the SAXS pattern. Also, when the samples were crystallized in situ by cooling from the melt at 10 °C/min, the crystallinity degrees were so small that no periodicities corresponding to lamellar stacking were observed (results not shown).

In the PE-*b*-PS system, depending on the volumetric fraction of the blocks, different morphologies were found and reported recently in a previous publication.[20] We have observed by TEM the morphology of $E_{53}S_{47}{}^{51}$, $E_{26}S_{74}{}^{105}$ and $E_{11}S_{89}{}^{244}$. The micrographs in Figure 1 show the typical lamellar, cylindrical, and spherical morphologies of the PE-*b*-PS system; morphologies that were observed after the crystallization of the PE block took place, i.e., no break-out occurred in this system as expected,[15] and this can be confirmed in the SAXS results that are shown in Figure 2.

The SAXS patterns observed for the PE-*b*-PS diblock copolymers at selected temperatures corresponding to the molten state (150 °C) and after controlled cooling (10 °C/min) to 25 °C are compared in Figure 2. The samples show characteristic reflections of the different morphologies revealed by TEM.[6] The higher order peak for the cylindrical morphology is broad. We speculate that it may either contain contributions from several higher order reflections or from the form factor. Also, it should noted that not all characteristic reflections of the cylinders and spheres are evident in Figure 2.

The ordered morphologies found in the molten state (Figure 2.i) remain after cooling to room temperature (Figure 2.ii). From the PE-*b*-PS *TEM* micrographs and SAXS patterns, we obtained the size (*l*) and the periodicity value (*d*) of the MDs for the PE-*b*-PS block copolymers (see Table 3). From this table, it can be seen that both experimental techniques yield similar values for the MDs dimensions.

2. Standard DSC Results. DSC cooling scans from the melt and subsequent heating scans are presented in Figure 3 for both diblock copolymer systems and for neat PE.[25] Also, Table 4 lists all relevant transition temperatures, enthalpies, and crystallinity degrees extracted from Figure 3.

Analyzing the crystallization behavior (see Figure 3a), a decrease in the crystallization temperature of the PE block was observed (in comparison with the PE homopolymer) as a function of the increasing length of the amorphous block (PS or PEP). It should be noted that the diluent effect of the PEP block decreases the crystallization temperature of the PE block to a greater degree than the presence of a PS block of similar length.

In the case of PE[25], $E_{53}S_{47}{}^{51}$, $E_{54}EP_{46}{}^{53}$, and $E_{29}EP_{71}{}^{99}$, the existence of a unique crystallization signal evidence that the crystallization process is due to heterogeneous nucleation. This is the typically observed behavior for polymers and for block copolymers if the crystallizable block forms a continuous phase (as a matrix or as a result of a percolation path).[8] For $E_{26}S_{74}{}^{105}$ (PE cylinders in a PS matrix) and $E_{11}S_{89}{}^{244}$ (PE spheres in a PS matrix) diblock copolymers, multiple crystallization exotherms are observed. This is caused by a fractionated crystallization phenomenon that is produced by the existence of different types of nucleation events, where each crystallization exotherm begins with a specific nucleation event (e.g., heterogeneous, superficial or homogeneous)[8,20] produced due to the

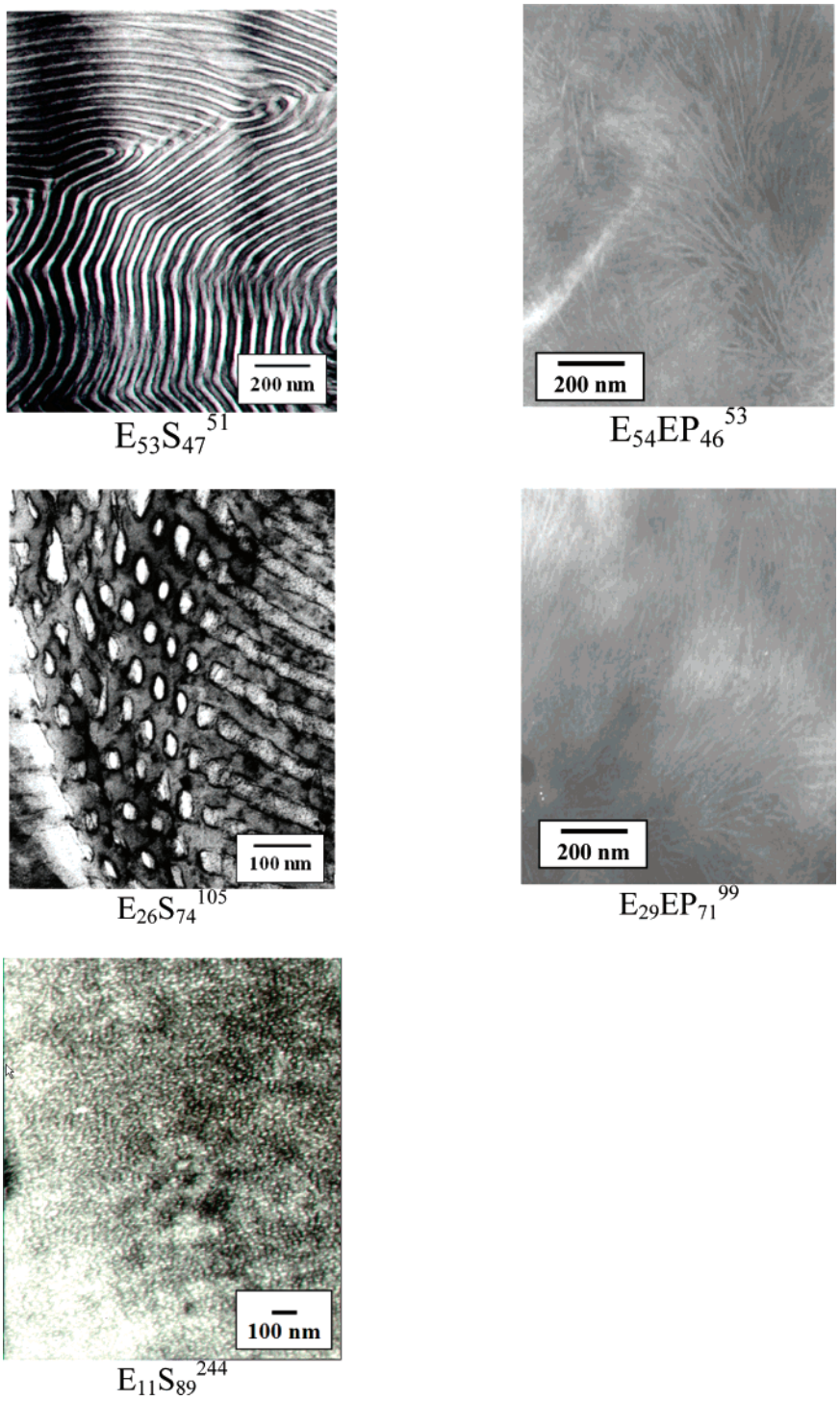

Figure 1. TEM micrographs of selected PE-*b*-PS and PE-*b*-PEP diblock copolymers. The diblock copolymers were stained with RuO_4.

high MDs density in comparison to the heterogeneities concentration usually present in an equivalent bulk sample of the crystallizable polymer. It was concluded for the $E_{11}S_{89}^{244}$, as the extreme case, that the lowest temperature crystallization signal (exothermic peak signal located at a T_c of 46.6 °C) could be originated from (a) superficial or interfacial nucleation events (due to the MDs interphase) or (b) from homogeneous nucleation events.[15] In this case, where polyethylene spheres are involved, we found the lowest temperature ever reported for the crystallization upon cooling from the melt of PE droplets so far.[20]

For the $E_{12}EP_{88}^{238}$ diblock copolymer (see Figure 3), two crystallization exotherms (fractionated crystallization) are observed which could originate from the existence of different nucleation events on the crystallization of the PE block. The higher temperature crystallization signal is probably originated by the nucleation of more active heterogeneities (i.e., usually available in bulk PE), but with a large depression on the T_c value due to the diluent effect of the PEP matrix. The existence of a certain fraction of the polymer crystallizing at a low temperature (second exotherm) could be caused by the high dilution offered by the PEP over the PE chains; if we consider that this diblock copolymer only contains 12 wt % of PE and just 17% crystallinity, this means that only about 2% of the overall block copolymer is capable of crystallizing within 98% of an amorphous matrix (a mixture between the amorphous PE and the PEP block). This could explain the case of extreme

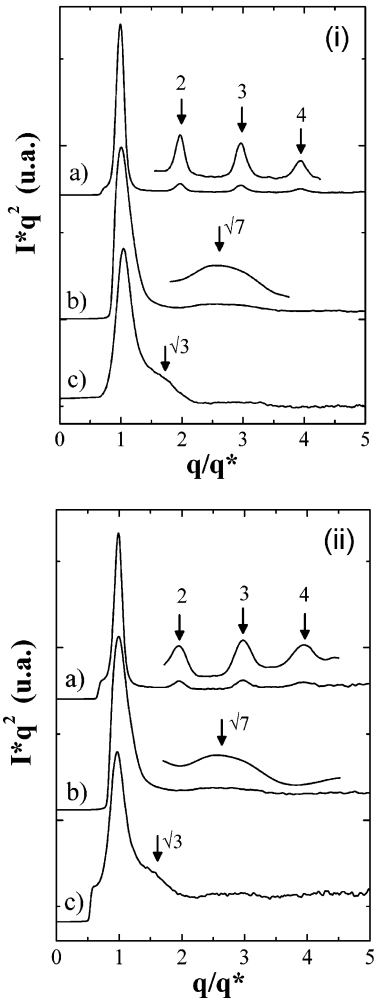

Figure 2. SAXS patterns recorded at (i) 150 and (ii) 25 °C (after a controlled cooling) for (a) $E_{53}S_{47}^{51}$, (b) $E_{26}S_{74}^{105}$, and (c) $E_{11}S_{89}^{244}$. Traces have been shifted vertically.

Table 3. Domain Size *l* and Spacing *d* of the PE-*b*-PS Diblock Copolymers As Determined by TEM and SAXS Measurements at Room Temperature

	TEM		SAXS	
copolymer	*l* (nm)	*d* (nm)	*d* (nm)	morphology
$E_{53}S_{47}^{51}$	16 ± 3^a	62 ± 3	65	lamellar
$E_{26}S_{74}^{105}$	21 ± 5^b	126 ± 29^c	99	PE cylinders
$E_{11}S_{89}^{244}$	12 ± 2^b	105 ± 13^c	108	PE spheres

[a] Thickness of the PE lamellae. [b] Radius of the microdomain. [c] Interdomain distance.

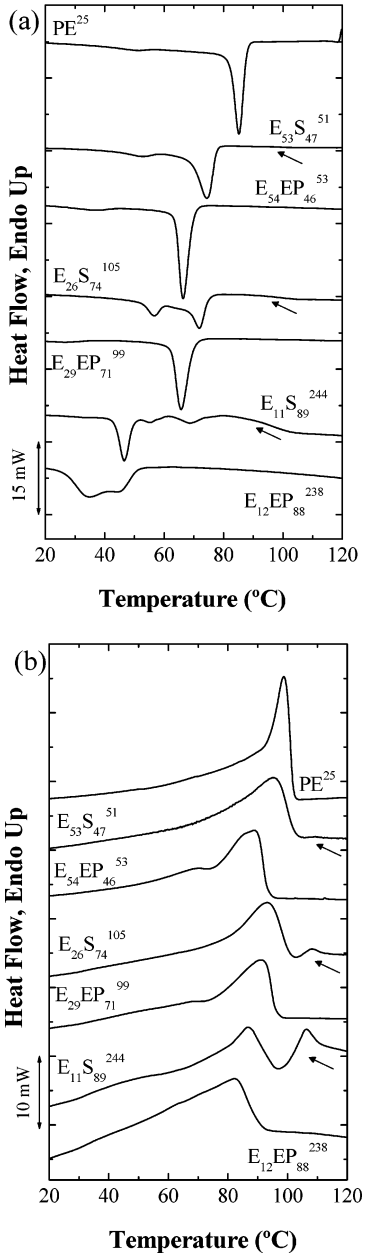

Figure 3. Cooling (a) and heating (b) *DSC* scans (10 °C/min) for the PE^{25} and the PE-*b*-PS and PE-*b*-PEP diblock copolymers studied. The curves were normalized as a function of the PE content within the block copolymers. The arrows indicate the glass transition signal for the PS block in the PE-*b*-PS copolymers.

dilution observed for this diblock copolymer and hence a similar isolated crystallization process of the dispersed PE phase. The depression of the melting temperature (see Table 4 and Figure 3) of $E_{12}EP_{88}^{238}$ cannot be explained only in terms of a diluent effect due to the compatibility of the two components in the melt. Morphological effects, at very low PE composition, must also be taken into consideration.

Figure 3b and Table 4 show that the PE^{25} homopolymer exhibits a peak melting temperature (T_m) of 98.7 °C. For the PE-*b*-PEP diblock copolymer, the diluent effect of the rubbery PEP block over the PE crystallization is clearly appreciable. We can observe (from Figure 3.b and Table 4) that the difference between the T_m values of the PE^{25} and the PE-*b*-PEP diblock copolymer is quite large. For example, we found a decrease (as compared to PE) of about 7 and 16 °C in the melting points of $E_{54}EP_{46}^{53}$ and $E_{12}EP_{88}^{238}$, respectively. This marked diluent effect could be associated with the miscibility of the amorphous PEP with PE due to similarity in the chemical structures of both blocks, expressed as a low interaction parameter between both blocks ($\chi_{E/EP} = 9.23 \times 10^{-3}$ at room temperature).[28,30]

Upon dissolving a crystallizable polymer in a low molar mass liquid, a depression of the melting temperature is observed which could be described by Raoult's law.[31] Generally, the melting point T_m of a lamellar polymer crystallite depends on its thickness *l*. Therefore, polymer crystallites with the same thickness will melt at a lower temperature if a diluent is present in the amorphous regions; however, this is not the only possible situation. If the diluent is present in the melt during the crystallization, this may well result in a thickness change, even if the crystallization temperature remains the same.[31] An analysis of melting point depressions therefore requires both knowledge of possible changes in the crystal thickness at a certain

Table 4. Thermal Properties of the Samples Studied

	T_c (°C)			ΔH_c (J/g)	$T_{m,peak}$(°C)	ΔH_m(J/g)	X_c (%)	T_g (°C)	solid state morphology
PE^{25}	85.2			−101	98.7	98	35		bulk
$E_{53}S_{47}^{51}$	74.4			−68	97.9	66	23	107.2	lamellar
$E_{26}S_{74}^{105}$	71.8	56.5		−54	93.0	54	18	107.2	PE cylinders
$E_{11}S_{89}^{244}$	68.7	55.6	46.6	−36	85.2	45	15	107.4	PE spheres
$E_{54}EP_{46}^{53}$	66.2			−79	91.3	76	27		lamellae
$E_{29}EP_{71}^{99}$	65.7			−77	88.7	73	27		lamellae
$E_{12}EP_{88}^{238}$		45.2	35.1	−54	82.4	30	17		

Table 5. T_s Temperatures Range for the Self-Nucleation Domains of Selected Materials

sample	domain I	domain II	domain III
PE^{25}	$T_s > 112$	$101 < T_s \leq 112$	$T_s \leq 101$
$E_{53}S_{47}^{51}$	$T_s > 116$	$99 < T_s \leq 116$	$T_s \leq 99$
$E_{54}EP_{46}^{53}$	$T_s > 113$	$94 < T_s \leq 113$	$T_s \leq 94$
$E_{29}EP_{71}^{99}$	$T_s > 114$	$94 < T_s \leq 114$	$T_s \leq 94$

crystallization temperature and the changes of the melting points during a subsequent heating.

The standard DSC results for the PE-*b*-PS diblock copolymers were extensively analyzed and discussed in a previous publication;[20] therefore, we are going to summarize briefly the conclusions obtained for these diblock copolymers. In the PE-*b*-PS diblock copolymers T_m does not change appreciably if the PE block forms a continuous or percolated phase ($E_{53}S_{47}^{51}$), as can be noted in Table 4. When the morphological confinement increases ($E_{26}S_{74}^{105}$ and $E_{11}S_{89}^{244}$), the T_m value decreases markedly (for $E_{11}S_{89}^{244}$ the T_m is 85.2 °C). A decrease in the melting temperature (and in the related fusion enthalpy) indicates that the previous crystallization process was more restricted inside each MD when the confinement increased as a result of increasing the PS content.

The DSC results analyzed in this section indicate that the crystallization of the PE block is affected by the covalent bond with the rubbery PEP block and the glassy PS block. A number of inferences can be drawn from the above analysis. The contrasting behavior of the two diblock copolymer systems seems to suggest that the mobility and miscibility of the amorphous PEP component markedly affect the crystallization and melting behavior of the PE block, in comparison with the immiscible and glassy PS block, where the topological restrictions given by the segregation in MDs (like lamellae, cylinders, and spheres) and the large number of MDs in the cylinder and the sphere morphology cases leads to fractionated crystallization.

3. Self-Nucleation Behavior. PE^{25}, $E_{53}S_{47}^{51}$, $E_{54}EP_{46}^{53}$, and $E_{29}EP_{71}^{99}$ diblock copolymers were found to exhibit a "classic" self-nucleation behavior. This was expected for the systems where the crystallizable component forms the matrix or the percolation level is high enough to allow the spread of secondary nucleation through all the PE crystallizable material, in an analogous way as it happens in the PE^{25} homopolymer and in commercial polymers. Table 5 shows the location of the self-nucleation domains of for PE^{25}, $E_{53}S_{47}^{51}$, $E_{54}EP_{46}^{53}$, and $E_{29}EP_{71}^{99}$.

When the diblock copolymers presented a fractionated crystallization, i.e., $E_{26}S_{74}^{105}$, $E_{11}S_{89}^{244}$, and $E_{12}EP_{88}^{238}$, a self-nucleation behavior was observed that totally differs from the "classic" behavior explained before. For example, the $E_{26}S_{74}^{105}$ diblock copolymer has two crystallization signals: (i) the higher temperature crystallization exotherm showed a "classic" behavior (with three SN domains), (ii) the second exotherm exhibited a direct transition from domain I to domain III_{SA}, a characteristic behavior exhibited by isolated MDs within block copolymers.[8,20,32−35] A complete analysis of the self-nucleation studies of the PE-*b*-PS diblock copolymers can be found in ref 36.

Like in the confined systems of the PE-*b*-PS diblock copolymers ($E_{26}S_{74}^{105}$ and $E_{11}S_{89}^{244}$) an atypical self-nucleation behavior was found for $E_{12}EP_{88}^{238}$. The higher temperature exotherm of this copolymer showed the three classic domains of self-nucleation, from domain I to II at 105 °C and from domain II to III at 88 °C. For the second crystallization exotherm the self-nucleation was even more restricted, therefore, a transition from domain I to domain III_{SA} was detected at 88 °C.[20,36] We can assume that the crystallizing PE chains are strongly isolated in the amorphous matrix (as explained, the amorphous matrix was about 98% of the material, formed by the mixture of amorphous PE and amorphous PEP), and therefore, the only way to inject the necessary self-nuclei is decreasing the T_s temperature to values where the domain III has already started.[8,20,32−36]

The self-nucleation of the samples corroborates the origin of the low-temperature exotherms exhibited by the materials when PE is present in isolated phases. Such low crystallization exotherms represent the crystallization of MDs that are isolated and therefore encounter nucleation difficulties.[8,20,32−36]

4. SSA. Figure 4 shows a comparison between the final heating DSC scans after SSA fractionation was performed to PE^{25} and to the PE block in the diblock copolymer samples with similar composition. The fractionated PE^{25} clearly shows a series of melting peaks that correspond to the melting of different mean lamellar thickness crystalline fractions that formed and annealed during the thermal protocol employed (see Experimental Part).[20,37] It is worth noticing that the short chain branching (SCB) distribution in PE^{25} (and in the PE block with the diblock copolymers) is totally random due to the synthesis procedure, and this explains the monomodal distribution of melting peaks observed.[37]

Figure 4 also shows how the highest temperature fraction of PE crystals is decreasing (or disappearing) due to the difficulties experienced by the PE chains when they have one end covalently bonded to a rubbery or glassy PEP or PS block, and the PE block tries to crystallize. The influence of the type of amorphous block (vitreous or rubbery at the PE block crystallization) in the SSA results of Figure 4 is very interesting. The dilution effect of the PEP on the PE crystallization has a stronger effect on the reduction of lamellar sizes produced by the SSA thermal treatment in the PE-*b*-PEP diblock copolymers than the PS confinement (topological restrictions) in the PE-*b*-PS for equivalent composition samples. Since no change in the distribution of SCB is present in the PE phase for all samples, all changes in the distribution of melting points (or lamellar thickness) must be accounted for by morphological restrictions of the vitreous PS or the diluent effect of the PEP on the PE chains.

The depression on the melting temperatures of the fractionated PE populations is greater in PE-*b*-PEP than in PE-*b*-PS diblock copolymers when a comparison with PE^{25} is performed. This implies that the diluent effect of the miscible PEP block on the thermal fractionation of the PE offers a stronger perturbation on the PE crystallization as compared to the case

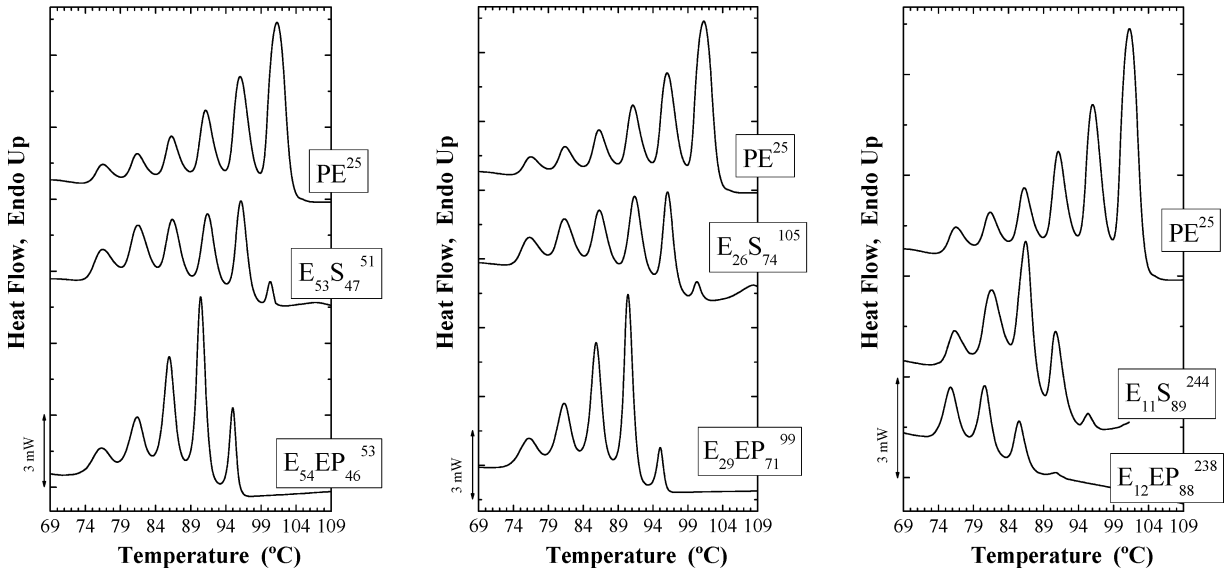

Figure 4. DSC final heating scans at 10 °C/min, after SSA thermal fractionation, for the PE^{25} and its comparison with PE-*b*-PS and PE-*b*-PEP diblock copolymers of similar composition.

when the PE is covalently bonded to PS and, therefore, strongly segregated.

In the PE-*b*-PS diblock copolymers, the differences that may be encountered in the thermal fractionation accomplished by SSA will be due to the topological restrictions on the PE block crystallization as the morphology changes from PE lamellae ($E_{53}S_{47}^{51}$) to PE spheres ($E_{11}S_{89}^{244}$). In general, a decrease in the high-temperature melting peak areas is observed as the content of PS increases in the PE-*b*-PS diblock copolymers.[20] At the same time, the low-temperature melting peak area usually increases.[20] The SSA results are fully consistent with the expectation based on the nonisothermal crystallization and melting behavior presented in Figure 3.

5. Isothermal Crystallization Analysis. DSC isothermal scans were recorded in order to study the crystallization kinetics of the PE block within the diblock copolymers after melting the samples for 3 min at 140 °C and quenching them (at 80 °C/min) to the desired crystallization temperature (T_c). After the crystallization was complete (the crystallization time was chosen as 3 times the experimental half crystallization time), a DSC heating scan was recorded from T_c until 140 °C with the purpose of obtaining melting traces of the isothermally crystallized PE block. The quality of the data obtained can be appreciated in Figure 5, where examples of isothermal DSC scans (Figure 5a) and the subsequent melting scans (Figure 5b) for the PE homopolymer are shown.

Figure 5b shows how the melting transition of the isothermally crystallized PE block forms a bimodal endotherm (T_m^1 and T_m^2). Double melting endotherms have been reported for many polymers and block copolymers and in particular for ethylene/α-olefin copolymers.[37−40] Alizadeh et al.[41] studied the double melting behavior of ethylene/1-octene copolymers and concluded that there was no apparent reorganization during heating in their samples and that the double melting effect was a direct reflection of two types of crystal families formed during the isothermal crystallization. Alizadeh et al.[41] and Crist et al.[42,43] have argued that the longest methylene sequences within random copolymers of ethylene and α-olefins can crystallize at the beginning of the crystallization forming thicker lamellae. At later times, shorter methylene sequences form the second crystal population which will have a lower melting point than the first population. In the present work, the hydrogenated

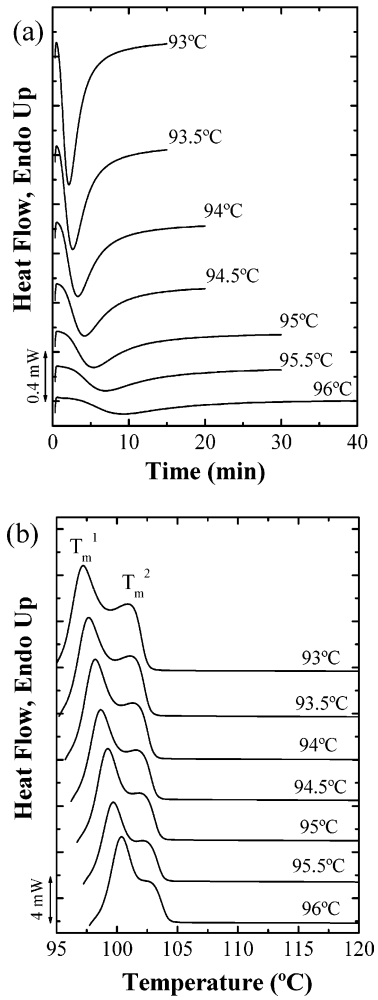

Figure 5. Examples of DSC isothermal crystallization scans (a) for the PE^{25} at selected crystallization temperatures and subsequent heating scans (b) (10 °C/min).

polybutadiene prepared by anionic polymerization also has a random distribution of short chain branching, as demonstrated above by SSA. Therefore, it is also possible that the melting of two types of lamellar thicknesses observed here could be due to the crystallization of different linear methylene sequences

within the short chain branching distribution of the hydrogenated polybutadiene.[20,37]

The data obtained from the isothermal crystallization of all the samples were initially analyzed with the Avrami equation[44−53]

$$1 - V_c(t) = \exp(-kt^n) \quad (1)$$

where V_c is the relative volumetric transformed fraction (i.e., relative amount of material that has crystallized), n is the Avrami index, and k is the overall crystallization rate constant (i.e., it contains contributions from both nucleation and growth). Equation 1 is the general Avrami relation, taking into consideration a constant nucleation rate and constant linear growth. A recent thorough review on the limitations and extensions of the Avrami theory has been published.[50] The analysis of the data was done applying the Avrami equation during the primary crystallization stage. We have employed a conversion range of 3−20% for all samples.

The crystallization phenomena of the PE block in the diblock copolymers under study can offer different behaviors: (i) when the PE is bonded to the PEP, the diluent effect can cause a significant delay of the crystallization kinetics, and (ii) in the strongly segregated PE-*b*-PS diblock copolymers, the PE chains are made to crystallize within a limited domain whose size can be, in magnitude, similar to the molecular chain size. It has been reported that the crystallization within the MDs surrounded by a glassy matrix can be greatly affected, since lower crystallinities are observed as well as thinner lamellar crystals.[18,19] This behavior has been recently reviewed by Müller et al.[8]

In order to perform the isothermal crystallization kinetics, samples were quenched to specific crystallization temperatures from the melt. The isothermal crystallization range is limited experimentally at higher temperatures by the long crystallization times encountered and at low crystallization temperatures by the impossibility to quench fast enough to prevent the polymer from crystallizing before the target T_c is achieved. We observed that, in general, the PE block covalently bonded to PEP blocks required much greater supercoolings to crystallize than those bonded to PS blocks of identical composition. In agreement with the SSA results, the dilution effect of the PEP block seems to affect to a greater extent the crystallization kinetics of the PE block, as compared to the topological restrictions exerted by the PS block.

From Figure 6 it can be noted that the Avrami index increases with T_c when the PE content within the diblock copolymers is 50% or higher (also for PE^{25}). Such a trend has been reported in the literature for PE and many other polymers, and it has been related to changes in the nucleation mechanism from instantaneous to sporadic nucleation when growth dimensionality is kept constant.[51] When PE is the minor phase within the diblock copolymers, the Avrami index is not so sensitive to changes in T_c.

Figure 6 also shows how the Avrami index exhibits a decreasing trend as the PE content in the diblock copolymers decreases. In other words, there is a clear correlation between a decrease in the Avrami index and an increase in the restrictions degree (morphological or from dilution) of the PE block within the copolymers. The shift in the crystallization temperature range is another evidence of the restrictions upon PE crystallization as indicated above, since the higher the confinement or dilution degree, the larger the supercooling needed to be applied in order to crystallize the PE block.

In the same order of ideas, Loo et al. applied time-resolved SAXS/WAXS to study crystallization in a range of PE-

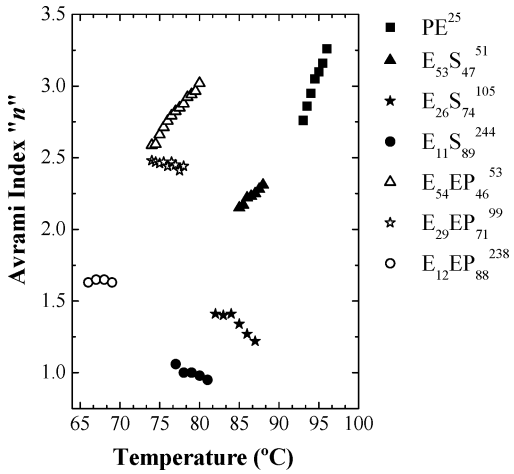

Figure 6. Avrami index values as a function of the isothermal crystallization temperature for the indicated PE-*b*-PS and PE-*b*-PEP diblock copolymers.

containing semicrystalline−glassy[18] and semicrystalline−rubbery[19] block copolymers, where the PE block formed spheres or cylinders. For the sphere-forming diblock copolymers, either in a glassy matrix (PE-*b*-PVCH 5/22, polyethylene-*block*-poly(vinylcyclohexane)) or in strongly segregated system (PE-*b*-PSEB 9/55, polyethylene-*block*-poly(styrene-*ran*-ethylene-*ran*-butene)), the progress of crystallization resulted in the observation of first-order kinetics ($n \sim 1$), therefore confirming confinement of the growing crystals by the isolated microdomains. Confined crystallization in cylindrical microdomains is also expected to result in first-order crystallization kinetics if these cylinders are not ''connected". Both glassy-matrix[18] PE-*b*-PVCH and strongly segregated[19] PE-*b*-PSEB diblocks forming PE cylinders indeed exhibited first-order crystallization kinetics. Nevertheless, Loo et al.[19] also demonstrated, after obtaining TEM images of PE-*b*-PMB 17/45 (polyethylene-*block*-poly(3-methyl-1-butene)) which showed occasional crystals traversing from one cylinder to another, that a single nucleus can crystallize the material initially in several cylinders, and this ''spreading" habit produces $n > 1$. This crystallization behavior was termed ''templated" crystallization, where the overall morphology of hexagonally packed cylinders is retained but the crystallization kinetics are sigmoidal, and the overall crystallization rate is faster than for analogous polymers (PE-*b*-PVCH and PE-*b*-SEB) where PE crystallization is completely confined, and each cylinder must be separately nucleated.

In the cases of the PE-*b*-PS diblock copolymers system, Takeshita et al.[54] found in their lamellar and cylinder-forming copolymers Avrami index values between 2.6−3.2 and 1.5−1.9, respectively. These values are quite similar to our Avrami values presented in Figure 6.

For the PE-*b*-PEP diblock copolymer system, the results about the crystallization of PE-PEE (ethylene-*block*-ethylethylene) found by Ryan et al.[29] could offer a good comparison. The PE-*b*-PEE diblock copolymer has a $T_{ODT} < T_m$, indicating that the crystallization of the PE block occurs from a homogeneous melt. Over a large range of PE volumetric fraction (0.25−0.75) the Avrami index was found to be near 3. In a similar way, Okamoto et al.[15] studied the crystallization kinetic behavior (from the disordered state) of a symmetric PE-*b*-PEP diblock copolymer; they found Avrami index values of about 3.0 ± 0.2 for all the crystallization temperatures evaluated.

Another interesting result shown in Figure 6 is that, for the cases where the PE block is highly confined, i.e., $E_{11}S_{89}^{244}$,

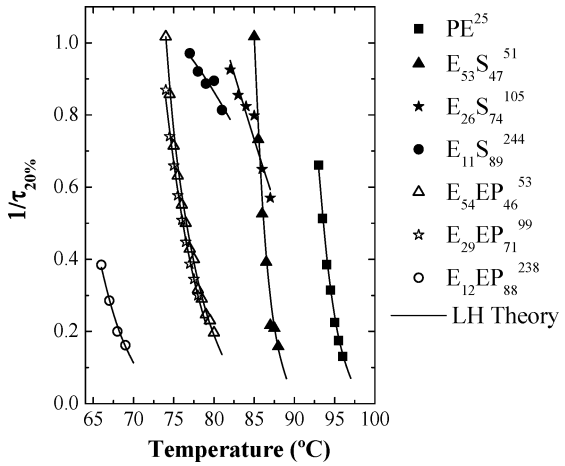

Figure 7. Variation of $1/\tau_{20\%}$ as a function of the crystallization temperature for the PE-*b*-PS and PE-*b*-PEP diblock copolymers.

Avrami indexes around 1 were obtained. We could infer, in this case, that crystallization starts from superficial or homogeneous nucleation phenomena because of the higher supercooling (as compared to other samples) needed for crystallization. It is well-known that when a polymer is confined within a high density of isolated MDs (i.e, spheres or cylinders), the probability for the superficial or homogenenous nucleation to occur increases.[8,20] Loo et al.[18,19] reported a simple exponential decay crystallization kinetics (i.e., $n \sim 1$) for polyethylene-*b*-poly(styrene-*ran*-ethylene-*ran*-butene) (PE-*b*-PSEB) diblock copolymers in which the PE blocks form isolated spheres or cylinders. From their work, it can be concluded that the crystallization kinetics strongly reflects the connectivity of the PE microdomains in such way that homogeneous (or superficial) nucleation and first-order kinetics were obtained for spheres or cylinders of PE, whereas conventional sigmoidal kinetics (i.e., $n > 1$) are obtained for the highly interconnected morphologies. The same conclusions were obtained many years ago for the crystallization kinetics of isolated polymer droplets vs bulk samples.[8,55,56] From a mathematical point of view, it can be established that when first-order kinetics are obtained using the Avrami fit, the crystallization rate has to be proportional to the fraction of crystallizable material not yet crystallized, i.e., that the crystal growth must be essentially instantaneous within isolated MDs. Then, the nucleation will be the rate-determining step in the crystallization process of isolated phases, like spheres or cylinders.[8,18,19]

For the $E_{26}S_{74}^{105}$ case, the Avrami index was found to be between 1.5 and 1.2. The Avrami index is an average value that reflects the characteristics of the nucleation event and growth dimensionality. In this case, for the $E_{26}S_{74}^{105}$, an important fraction of the PE block is confined in cylindrical MDs for which an Avrami index value of 1 is expected (since nucleation will be the determining overall rate transformation step). Nevertheless, if a fraction of the cylinders population is percolated, as it is probably the case here, it is also possible that crystal growth gains more importance, increasing slightly the Avrami Index to a value near 1.5, as it was found.[8,18,19]

We have employed the inverse of $\tau_{20\%}$ (i.e., the time needed for 20% relative crystallization) as a measure of the crystallization rate in order to analyze its dependence on the crystallization temperature (see Figure 7).[51−53,57−58]

The interpretation of the inverse of $\tau_{20\%}$ as an overall crystallization rate must be performed with great caution in the systems under study since they are subject to very different conditions such as confinement, dilution, and widely different Avrami indexes. Since PE is a highly flexible polymer, its crystallization window extends in a wide range from its equilibrium melting temperature (145.5 °C for linear PE and 125.9 °C for the hydrogenated polybutadiene employed here) to its glass transition temperature (a controversial value that is considered by some authors to be around −120 °C and by others approximately −20 °C).[21] This means that the crystallization window in the present case "if we take the T_g to be −20 °C" extends over 166 °C. The lowest T_c employed was 66 °C for $E_{12}EP_{88}^{238}$; therefore, our experimental isothermal crystallization range is very far from T_g, especially when compared with studies performed in less flexible polymers where crystallization temperatures close to T_g can be employed (in such temperatures diffusion or transport to the crystallizing front will be important).[59]

Five cases can be considered: (a) Percolated systems where the PE block is not in isolated MDs such as PE-*b*-PEP diblock copolymers of composition $E_{54}EP_{46}^{53}$ and $E_{29}EP_{71}^{99}$ or those compositions of PE-*b*-PS where the PE block conforms the matrix (i.e., $E_{53}S_{47}^{51}$). For these systems, the overall crystallization most probably proceeds via nucleation and growth. (b) Systems with isolated MDs that can be represented by PE spheres within a PS matrix like in $E_{11}S_{89}^{244}$. In this case, the overall crystallization kinetics will be dominated by primary nucleation since the growth within such nanodroplets can be considered instantaneous. (c) The block copolymer that forms PE cylinders within a PS matrix; i.e., $E_{26}S_{74}^{105}$ can be considered an intermediate case since it contains a fraction of percolated cylinders and a fraction of isolated cylinders, and its fractionated crystallization process is a reflection of the mixture of these two crystal populations. (d) The special case of $E_{12}EP_{88}^{288}$ should be considered. Since its PE content is so low, the PE chains are molecularly confined by the excess PEP chains that can also be considered a macromolecular solvent (that causes extreme dilution). In this final case both confinement and dilution of PE chains are present. (e) Finally, the rest of the PE-*b*-PEP cases, where dilution of PEP on PE is encountered without any PE confinement.

Because of the different situations encountered, the isothermal crystallization kinetics data have been analyzed with a variety of models in order to quantify the energy barriers as a function of the diblock copolymer composition.

The first theory to be considered is that of Lauritzen and Hoffman which provides expressions for the linear growth rate (originally of spherulites, axialites or single crystals) as a function of supercooling. The theory assumes that the lateral growth rate (g) is equal to the microscopically observed growth rate (G). The secondary or tertiary nucleation and its respective rate (i) together with the short range diffusion of the crystallizable units controls the growth rate. Experimental results show that the growth rate is proportional to $\exp(-1/\Delta T)$, and the formation of facetted single crystals in solution has been employed as evidence that polymer crystallization is nucleation controlled[60,61] although recent evidence challenges such a view, and the application of the LH model is under review.[62] The growth rate can be expressed as[51,60,61]

$$G(T) = G_0 \exp\left(\frac{-U^*}{R(T_c - T_\infty)}\right) \exp\left(\frac{-K_g}{T_c \Delta T_f}\right) \qquad (2)$$

where G_0 is a growth rate constant, U^* is the activation energy for the transport of the chains to the growing nuclei (a value of 1500 cal/mol is normally employed), R is the gas constant, and T_c is the isothermal crystallization temperature. T_∞ is a tem-

perature at which chain mobility ceases, and it is usually taken as $T_g - 30$ (K). ΔT is the supercooling defined as $(T_m^0 - T_c)$, where T_m^0 is the equilibrium melting point. The factor f is a temperature correction term equal to $2T_c/(T_c + T_m^0)$, and K_g is a secondary nucleation constant, which is proportional to the energy barrier for secondary nucleation.

The second term of the right-hand side of the LH equation (eq 2) adopts the form of the Vogel−Fulcher−Tamman−Hesse (VFTH) equation which describes the nonlinear long-range diffusion behavior in the temperature region close to T_g using parameters U^* and T_∞. Finally, the third term on the right-hand side of eq 2 describes the nucleation rate and depends on the undercooling ($\Delta T = T_m - T_c$). The parameter K_g is the secondary nucleation constant and has the following expression:

$$K_g = \frac{jb_0\sigma\sigma_e T_m^0}{k\Delta h_f} \tag{3}$$

where k is Boltzmann's constant. The parameter j varies with regime: $j = 4$ in regimes I and III and $j = 2$ in regime II. Therefore, it can be predicted that $K_{g(I)} = K_{g(III)} = 2K_{g(II)}$, which is an important criterion for the LH theory. σ is the lateral surface free energy, σ_e is the fold surface free energy, and Δh_f the heat of fusion of a perfect crystal. The K_g values can be determined by plotting $\ln G + U^*/R(T_c - T_\infty)$ vs $1/T_c\Delta T$, making the so-called LH plot. The product of surface free energy $\sigma\sigma_e$ can be calculated from K_g, and the following expressions allow the calculation of σ (and σ_e) and q, the work done by the chain to form a fold:

$$\sigma = 0.1\Delta h_f\sqrt{a_0 b_0} \tag{4}$$

$$q = 2a_0 b_0 \sigma_e \tag{5}$$

where a_0 and b_0 correspond to the projected chain length and chain width, respectively, within the crystal.

Although the LH theory successfully predicts the undercooling dependence of growth rate, the regime transition behavior, and the undercooling dependence of the lamellar thickness, there are still several problems associated with this theory: (i) The LH theory neglects the fluctuations in lamellar thickness, and recent morphological evidence suggests that rough surfaces may be encountered during growth as opposed to smooth surfaces assumed by the theory (notably by atomic force microscopy[63]). (ii) In the LH theory, the stems deposited on the substrate have a fixed length, and the substrate completion step is very fast and weakly dependent on the undercooling. (iii) The LH theory only considers the free energy difference between the states before and after deposition.

Even though the LH treatment was developed for describing crystal growth only, it has been employed to describe overall crystallization data since it is capable of fitting the data remarkably well.[57] In these cases, such as when isothermal crystallization kinetics data obtained by DSC are employed, the energy barrier for crystallization reflected in the K_g value contains contribution from both primary nucleation and growth.

In a previous work, Müller et al.[58] studied the overall crystallization kinetics of poly(ϵ-caprolactone), PCL, poly(*p*-dioxanone), PPDX, and PPDX-*b*-PCL diblock copolymers by DSC in neat and self-nucleated samples while spherulitic growth rates were determined by polarized light optical microscopy (PLOM); an excellent correlation was found between the values of K_g obtained by the LH treatment from spherulitic growth rate data and those measured in self-nucleated samples by DSC. It was concluded that the self-nucleation treatment was 100% efficient, and therefore the data obtained by DSC contain information on crystal growth only; hence, identical values of K_g were obtained. In samples that were not self-nucleated the K_g values obtained by the LH treatment from DSC data were much larger than those obtained by PLOM; this was explained by the contribution of both primary nucleation and growth on the former values.

Table 6. Values Obtained by Fitting the Lauritzen−Hoffman to DSC Isothermal Experimental Data and Calculated with Eqs 4 and 5[a]

compolymer	K_g^r **(K^2)**	σ *(*erg/cm^2*)*	σ_e (erg/cm^2*)*	q (kcal/mol)
PE[25]	2.27×10^5	12.78	218.1	11.8
PE[25] sn 103 °C	1.66×10^5	12.78	156.2	8.6
$E_{53}S_{47}$[51]	4.29×10^5	12.78	410.9	22.3
$E_{26}S_{74}$[105]	9.15×10^4	12.78	87.8	4.8
$E_{11}S_{89}$[244]	7.04×10^4	12.78	67.5	3.7
$E_{54}EP_{46}$[53]	3.05×10^5	12.78	292.8	15.9
$E_{29}EP_{71}$[99]	3.14×10^5	12.78	301.5	16.4
$E_{12}EP_{88}$[238]	4.96×10^5	12.78	475.5	25.8

[a] Constant values employed: $T_\infty = -60$ °C; $\rho_{am-PE} = 0.887$ g/cm^3; $\rho_{cr-PE} = 0.999$ g/cm^3; $a_0 = 0.455$ nm; $b_0 = 0.415$ nm; $\Delta H^0 = 293$ J/g; $T_m^0 = 125.9$ °C.[23] sn = self-nucleated material at the indicated T_s temperature; see text. Errors in K_g^r are estimated to be less than 3%.

On the basis of the results of the previous work described above, we decided to employ the LH treatment on DSC data taken for both PE homopolymer and the PE block within PE-*b*-PS and PE-*b*-PEP. However, in the present case, we were not able to measure spherulitic growth rates by PLOM because the spherulites were either too small (in the PE homopolymer case and in block copolymers where PE was the matrix) or nonexistent (in those PE-*b*-PS diblock copolymers with PE contents lower than 70%). Nevertheless, with the purpose of quantifying the energy barrier corresponding to crystal growth only in PE homopolymer, self-nucleation experiments were performed in this polymer immediately followed by isothermal crystallization. Therefore, in the PE homopolymer case, we have K_g values determined by DSC in neat samples (reflecting primary nucleation and growth) and in self-nucleated samples (reflecting growth only). We have assumed that the difference in these two K_g values gives an idea of the K_g value for primary nucleation only.

Figure 7 shows how the Lauritzen and Hoffman theory was applied to fit overall crystallization kinetics data $1/\tau_{20\%}$ for the PE-containing diblock copolymers and also for PE[25]. We have initially assumed that crystal growth occurs under regime II, and the values of all parameters employed for the calculation are listed in Table 6; the possibility that the crystallization process was under regime III in those diblock copolymers with 20 wt % PE or less will be analyzed in the following paragraphs.

It was shown that as the PE chains become more confined or diluted by increases in PS or PEP content, respectively, the supercooling needed for the crystallization process also increases, indicating the larger thermodynamic driving force needed for crystallization of the PE chains in both systems. This trend is clearly seen in Figure 8, where $1/\tau_{20\%}$ values have been plotted as a function of supercooling. The supercooling represented in Figure 8 was obtained with a value of the equilibrium melting point calculated by Flory's equilibrium theory for copolymer melting:[37,51,64]

$$\frac{1}{T_{m,c}^0} - \frac{1}{T_m^0} = \frac{-R}{\Delta h_u}\ln p \tag{6}$$

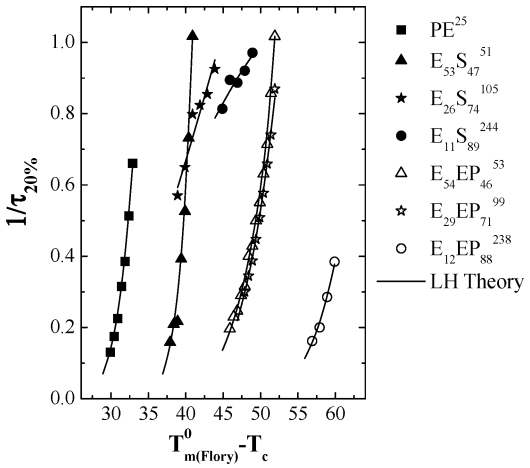

Figure 8. Variation of $1/\tau_{20\%}$ as a function of the supercooling degree ($T^0_{m(Flory)} - T_c$) for PE-*b*-PS and PE-*b*-PEP diblock copolymers.

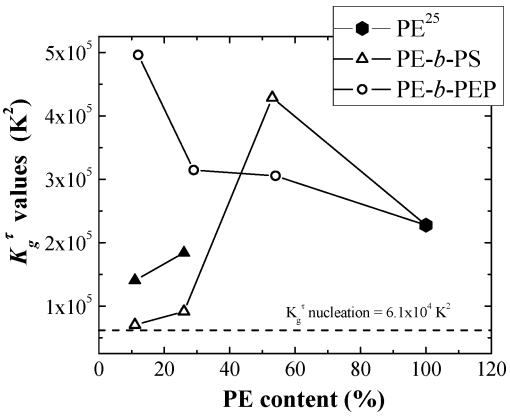

Figure 9. Variation of K_g^τ (regime II) as a function of the PE content within the diblock copolymers. Filled triangles represent K_g^τ values calculated employing regime III growth.

where $T^0_{m,c}$ is the equilibrium melting temperature of the copolymer, T^0_m is the equilibrium melting temperature for linear polyethylene, i.e., 145.5 °C, R is the universal gas constant, $\Delta h_u = 960$ cal/mol, and $p = X_A$ (in this case, the molar fraction of ethylene for a random copolymer of ethylene and an α-olefin). The value of the equilibrium melting temperature for PE[25] according to eq 6 is 125.9 °C. This value was employed as a constant for PE[25] and all the PE blocks within the copolymers for the purposes of representing Figure 8 and for the fittings of the Lauritzen and Hoffman theory.

From Figure 8 it can be concluded that in the PE-*b*-PS copolymers where confinement is very large (cylinders and spheres) the overall crystallization rates are strongly affected as shown by the large values of $1/\tau_{20\%}$ at maximum supercooling (for this system) and, as was explained before, Avrami indexes approaching unity.

Also, from Figure 8 it can be noted how the diluent effect of the PEP block has a stronger depressing effect upon the PE crystallization kinetics than the PS block in the analogous PE-*b*-PS diblock copolymers, since higher supercooling values are needed (for similar compositions in both diblock copolymer systems) in order to crystallize the PE chains. Since the LH treatment does not consider dilution effects, we have also employed a modified treatment by Boon and Azcue[65] to be commented later. Table 6 shows the values obtained by fitting the LH theory to the DSC isothermal data of the PE[25] and the PE block within the diblock copolymers studied.

From Table 6 and Figure 9 it can be seen how K_g^τ values (the superscript τ indicates that the values were determined by DSC employing $1/\tau_{20\%}$ as a measure of crystallization rate) for the PE block within PE-*b*-PEP increase progressively (in comparison with the value found for the PE[25]) as the PEP content increases. The K_g^τ values are consistent and confirm the trends about the diluent effect found in standard crystallization and SSA thermal fractionation behavior for these diblock copolymers. As a result of the increases in K_g^τ, the values of fold surface free energy and the work to fold the PE chains also increase in a similar way.

The PE-*b*-PS diblock copolymers exhibit a more complex behavior; for those PE compositions where the percolation degree is high (i.e., $E_{53}S_{47}$[51]) the energy barrier for the crystallization process increases with the PS content; however, when the PE block is confined in MDs, i.e., $E_{26}S_{74}$[105] and $E_{11}S_{89}$[244], K_g^τ decreases markedly to very low values in comparison with the value obtained for PE.[25] In order to understand this interesting behavior, it should be remembered that the Avrami index was found to be between 1.5 and 1 for these diblock copolymers, a result which indicates that crystal growth must have been essentially instantaneous within isolated MDs and the nucleation event was the rate-determining step in the overall crystallization.

The K_g^τ value represents the energetic barrier for the crystallization phenomena to occur. It involves two events since it was determined from overall crystallization kinetics data: nucleation and growth. In order to assess the relative contributions of nucleation and growth to the overall kinetics, the self-nucleation technique was applied to PE[25] before isothermal crystallization. The sample was first self-nucleated (at 103 °C) and then quenched (at a controlled cooling rate of 80 °C/min) to its isothermal crystallization temperatures. Since the self-nucleation treatment provides in principle all nuclei needed, the kinetics determined after self-nucleation should correspond to growth only (see ref 58).

The results are very satisfactory since the K_g^τ value obtained for the PE[25] is reduced from 22.7 to 16.6 ($\times 10^4$ K^2) once the self-nucleation step is performed before the isothermal crystallization (see Table 6). This indicates that the energy barrier for nucleation is about 6.1×10^4 K^2; in other words, it represents only 25−27% of the K_g^τ value obtained for the isothermal crystallization of the PE[25] in the standard way. This experiment performed on PE[25] allows us to obtain an idea of the order of magnitude of the energetic barrier associated with PE nucleation, a value which may be used as a reference for the possible minimum value of the nucleation barrier of the PE blocks within the diblock copolymers employed here. This value of 6.1×10^4 K^2 is of the same order of magnitude (see dashed line in Figure 9) as the energy barrier for the overall crystallization process of the PE block within $E_{26}S_{74}$[105] and $E_{11}S_{89}$[244], whose K_g^τ values are (see Table 6) 9.1×10^4 and 7.0×10^4 K^2, respectively. This coincidence in the orders of magnitude of these values suggests that during the overall isothermal crystallization of the PE blocks within $E_{26}S_{74}$[105] and $E_{11}S_{89}$[244] the rate-determining step is the nucleation event, as expected for isolated MDs solidification.

Therefore, the reason why the K_g^τ values suddenly decrease in Figure 9 as the PS content increases in PS-*b*-PE is that the kinetics are changing from nucleation and growth control to just nucleation control, in view of the isolation of the MD's into spheres and cylinders.

Since nucleation is the rate-determining step in the overall crystallization of the isolated phases within $E_{26}S_{74}$[105] and $E_{11}S_{89}$[244], the preponderance of regime II has to be reconsidered.

Table 7. Values Obtained by Fitting the DSC Isothermal Experimental Data of the PE-*b*-PS Block Copolymers to Different Crystallization Theory Approaches

copolymers	K_g^{τ} (K^2)	R^2	E_a (K min^{-1})	R^2	k_2 (K min^{-1})	R^2	k_3 (K min^{-1})	R^2
PE^{25}	2.27×10^5	0.9986	530	0.9992	526	0.9985	20	0.9983
$E_{53}S_{47}^{51}$	4.29×10^5	0.9836	992	0.9846	966	0.9849	47	0.9839
$E_{26}S_{74}^{105}$	9.15×10^4	0.9857	161	0.9831	140	0.9837	7	0.9844
$E_{11}S_{89}^{244}$	7.04×10^4	0.9833	84	0.9785	97	0.9928	5	0.9914

It could be argued that a more suitable approach would be to consider that for these copolymers the crystallization occurs within regime III. In regime III, the nucleation rate is high as compared to the growth rate, since many nucleation sites are created at the melt−crystal interphase. In the case of confined PE domains, the situation is different since the domains are physically isolated and the supercoolings employed are not as high as those generally involved in regime III. In other words, in the absence of confinement the supercooling alone may not guarantee such a prolific nucleation. Nevertheless, the effect of considering such a change only implies a change in a factor of 2 in the K_g^{τ} value in Table 6. Given the orders of magnitude involved, the argument of nucleation being the rate-determining step would still hold for the isolated phases independently of the growth regime under consideration. To illustrate this last remark, two extra data points calculated with regime III growth for the sphere and cylinder cases of PS-*b*-PE have been also plotted in Figure 9 (filled triangles).

The above argumentation could shed doubts on weather the LH theory is applicable for confined samples where nucleation could be the dominant step in the kinetics. Therefore, theories that consider only primary nucleation have also been employed to fit the data, and the results are presented in Table 7 and in the following paragraphs. Two cases of nucleation in the vicinity of T_m^0 have been considered: (1) for three-dimensional nucleation $N(T)$ is proportional to $(1/\Delta T^2)$ (see eq 7) and (2) for two-dimensional nucleation $N(T)$ is proportional to $(1/\Delta T)$ (see eq 8).[51]

$$N(T) = N_0 \exp\left[\frac{-E_D^*}{RT} - \frac{k_3(T_m^0)^2}{T(\Delta T)^2}\right] \quad (7)$$

$$N(T) = N_0 \exp\left[\frac{-E_D^*}{RT} - \frac{k_2 T_m^0}{T\Delta T}\right] \quad (8)$$

where E_D^* is the activation free energy for the short-range movement of molecules crossing the interfacial boundary in order to join the nucleus. The constants k_3 and k_2 are complex quantities that contain information about the geometry of the nucleus, whether it is formed by homogeneous or heterogeneous nucleation, and the enthalpy of fusion per repeating unit.

Mandelkern[51] argues that it is very difficult to ascertain whether two- or three-dimensional nucleation is operative. Figure 10 shows fittings of isothermal crystallization data collected for $E_{11}S_{89}^{244}$, where isolated spheres crystallize within a glassy PS matrix. Four plots are shown corresponding to the LH treatment, two-dimensional nucleation, three-dimensional nucleation, and a simple Arrhenius-type plot based on the following equation:

$$1/\tau(T) = A_0 \exp\left(\frac{E_a}{\Delta T}\right) \quad (9)$$

where A_0 is a pre-exponential constant and E_a is a activation energy value.

The agreement between the fits and the data in Figure 10 is very good in all four cases ($R^2 > 0.98$), and from the slopes, values that are proportional to complex energy barrier terms have been calculated and are reported in Table 7. A similar good fit was obtained for all the diblock copolymer samples employed here, and the final trends for the energy terms (i.e., slope of all plots prepared as in Figure 10) followed exactly the same pattern as in Figure 9.

Figure 10 and Table 7 demonstrate that, regardless of the theory employed, similar trends to that exhibited by K_g^{τ} as a function of composition in Figure 9 are obtained when k_2 or k_3 or even the Arrhenius activation energy is considered. (These parameters cannot be quantitatively compared in view of their different units and conceptual differences.) The rationale behind these results is that the isothermal crystallization temperatures employed are much higher than T_g, and therefore the crystallization process can be considered to be carried out close enough to the equilibrium melting temperature that the temperature variation of the activation energy in the transport terms (long and short range) is small. However, the fact remains than when the PE is confined into cylinders and spheres, a dramatic change in overall crystallization kinetics occurs.

Summarizing the results obtained after applying different kinetic theories of polymer nucleation and crystallization to our data, we have observed that in the cases where the PE block is covalently bonded to a strongly segregated PS block, the behavior obtained is complex. If the PE block is well percolated (as when it conforms the matrix or lamellae), the energy barrier associated with the overall crystallization increases with the increase in PS content. On the contrary, when the PE chains are within isolated MDs, such as cylinders or spheres, the energy barrier decreases with the degree of confinement, since the energy penalization associated with crystal growth decreases as the nucleation becomes the rate-determining step.

In the PE-*b*-PEP diblock copolymers, the crystallization kinetics for $E_{54}EP_{46}^{53}$ and $E_{29}EP_{71}^{99}$ are quite similar (see Figure 8); this reflects that the diluent effect, offered by the mixture of PEP amorphous block plus PE amorphous phase, reaches a saturation level. The crystallization kinetics of $E_{12}EP_{88}^{238}$ are affected by the diluent effect of the PEP block and by an indirect confinement upon the PE block (due to its low content in the sample), where the PE chains are incapable of establishing efficient percolation routes in order to promote the PE crystallization (see Figure 9 and Table 6).

In the case of the PE-*b*-PEP block copolymers we need to consider the diluent effect of the PEP block upon the PE crystallization. The results presented in Table 7 and Figure 9 demonstrate that the energy barrier associated with the overall isothermal crystallization of PE block increases when it is covalently bonded to a PEP miscible block, and its value increases as the PEP content within the copolymer increases. Such an energy barrier increase can be physically understood since the availability of chains in the growing front decreases as the system is diluted with miscible PEP chains. Boon and Azcue[65] developed a modification for the theory of polymer crystallization of Turnbull and Fisher to describe the effect of the low molecular weight diluent benzofenone on isotactic polystyrene. We have also applied this model to the PE-*b*-PEP diblock copolymers considering PEP as a macromolecular

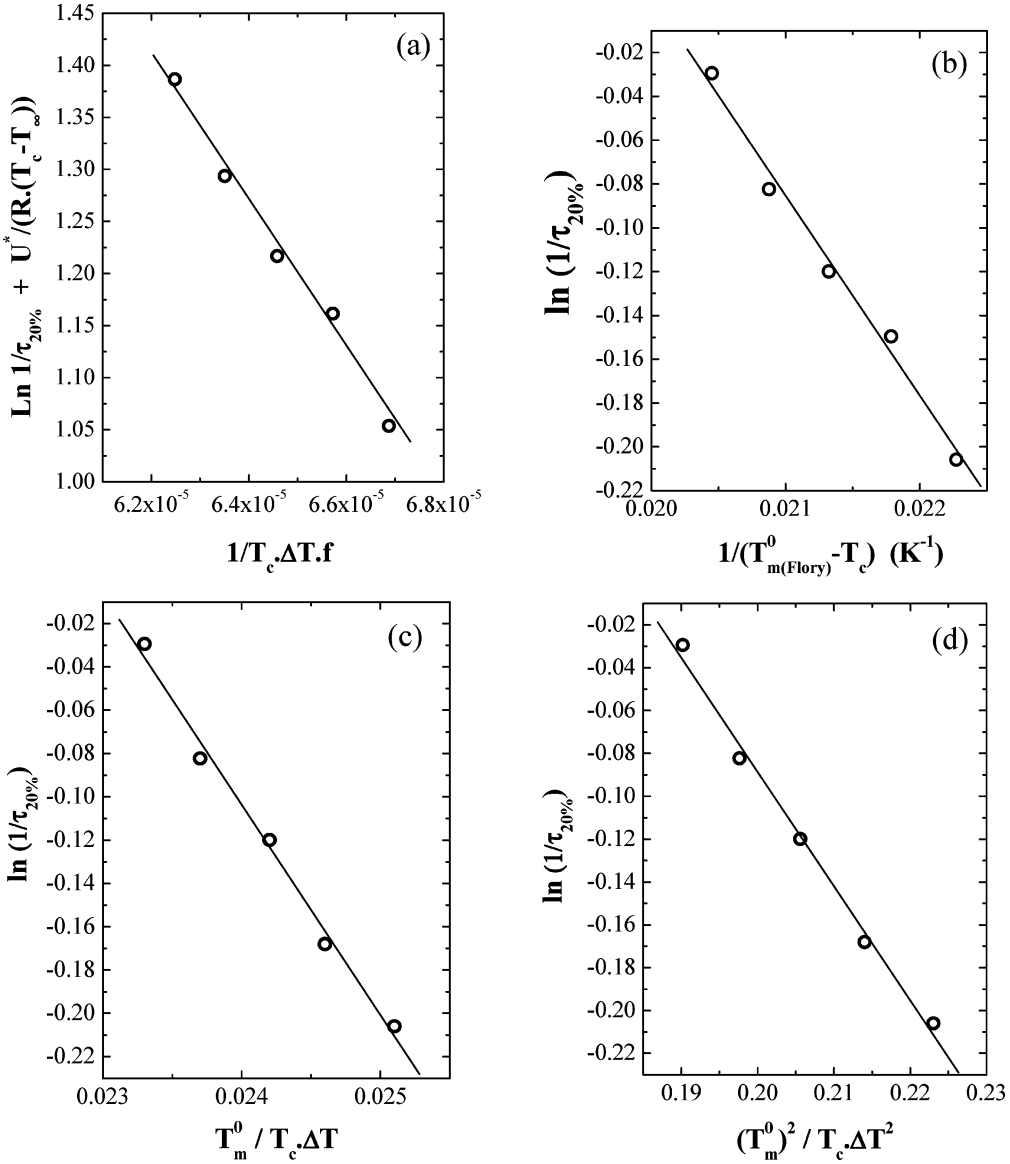

Figure 10. Fittings of isothermal crystallization data collected for $E_{11}S_{89}^{244}$. Four plots are shown corresponding to (a) the LH treatment, (b) Arrhenius-type plot, (c) two-dimensional nucleation, and (d) three-dimensional nucleation.

diluent, but the results obtained were qualitatively very similar to those obtained employing the LH treatment and summarized in Figures 8 and 9.

Conclusions

The crystallization processes of model PE blocks were compared when they are covalently bonded to rubbery PEP blocks and vitreous PS blocks. Confinement effects and topological restrictions on the PE block are enhanced as the PS content in the copolymers increases, causing a decrease in both the crystallization and melting temperatures of the PE block crystals, as indicated by DSC, TEM, and SAXS evidence. When the PE is confined into cylinders or spheres, a fractionated crystallization phenomenon is induced by the excess MD density as compared to the available number density of nucleating heterogeneities. In contrast, when PE is covalently bonded to PEP, a strong diluent effect is observed upon PE crystallization, and in the extreme case of $E_{12}EP_{88}^{238}$, fractionated crystallization was also observed for the PE block. Additionally, the difference between bonding to a rubbery block and bonding to a glassy block was obtained by successive self-nucleation and annealing (SSA), and the results showed that the dilution effect of PEP can cause even stronger effects on the depletion of higher melting thermal fractions than the confinement effect of PS.

Several classical polymer nucleation and crystallization kinetic theories were applied to overall DSC isothermal crystallization rate data. The results indicate that the energetic restrictions for the crystallization of the PE block increase as the PE content in the PE-*b*-PEP diblock copolymers decreases.

The behavior of the PE-*b*-PS system is more complex. If the PE block is well percolated (as when it conforms the matrix or lamellae), the energy barrier associated with the overall crystallization increases with the increase in PS content. On the contrary, when the PE chains are within isolated MDs, such as cylinders or spheres, the energy barrier decreases with the degree of confinement, since the energy penalty associated with crystal growth decreases as the nucleation becomes the rate-determining step. In such extreme confined cases, $E_{26}S_{74}^{105}$ and $E_{11}S_{89}^{244}$, it was demonstrated, by applying the Lauritzen−Hoffman theory to data from DSC measurements of isothermal crystallization of previously self-nucleated PE, that the crystallization behavior was mostly determined by the nucleation process rather than by crystal growth, since for these compositions an important depression of the K_g^{τ} value was detected as compared to PE

homopolymer or the other compositions where PE was the excess component. These results are in agreement with the low Avrami index values found for these diblock copolymers ($n < 1.5$). When nucleation theories were applied to the same data, similar qualitative trends were found.

Acknowledgment. Synthesis of the polymers was carried out at the University of Bayreuth. A.T.L. and A.B. acknowledge financial support by Deutsche Forschungsgemeinschaft (SFB 481) during their time in Bayreuth. Further support was given by Fonds der Chemischen Industrie and the Hasylab Project II-20052048. The USB team acknowledges financial support from Fonacit and USB through Grants G97-000594 and DID-GID-02. The authors thank Daniel Fierro and Julio Albuerne for their help with SAXS measurements.

References and Notes

(1) Brown, R. A.; Masters, A. J.; Price, C.; Yuan, X. Chain Segregation in Block Copolymers. In *Comprehensive Polymer Science—The Synthesis, Characterizations, Reaction & Applications of Polymers*, 1st ed.; Aggarwal, S., Ed.; Pergamon Press: London, 1989; Vol. 7, pp 155−197.
(2) Hadjichristidis, N.; Pispas, S.; Floudas, G. In *Block Copolymers: Synthetic Strategies, Physical Properties, and Applications*, 1st ed.; Wiley-Interscience: London, 2002.
(3) Cowie, J. M. G. Carbon-Chain Block Copolymers and Their Relationship with Solvents. In *Developments in Block Copolymers*, 1st ed.; Applied Science Publishers: London, 1982; pp 1−37.
(4) Abetz, V. Block Copolymers. In *Encyclopedia of Polymer Science and Engineering*; John Wiley & Sons: New York, 2001; pp I−LV.
(5) Abetz, V. Assemblies in Complex Block Copolymer Systems. In *Supramolecular Polymers*; Marcel Dekker: New York, 2000; Chapter 6.
(6) Hamley, I. W. In *The Physics of Block Copolymers*; Oxford University Press: London, 1998.
(7) Müller, A. J.; Balsamo, V.; Arnal, M. L. In *Lecture Notes in Physics: Progress in Understanding of Polymer Crystallization*; Reiter, G., Strobl, G., Eds.; Springer: Berlin, Germany; *Lect. Notes Phys.* **2007**, *714*, 229.
(8) Müller, A. J.; Balsamo, V.; Arnal, M. L. *Adv. Polym. Sci.* **2005**, *190*, 1.
(9) Quiram, D. J.; Register, R. A.; Marchand, G. R. *Macromolecules* **1997**, *30*, 4551.
(10) Quiram, D. J.; Register, R. A.; Marchand, G. R.; Ryan, A. J. *Macromolecules* **1997**, *30*, 8338.
(11) Bodganov, B.; Vidts, A.; Schacht, E. *Macromolecules* **1999**, *32*, 726.
(12) Rangarajan, P.; Register, R. A.; Fetters, L. *Macromolecules* **1993**, *26*, 4640.
(13) Rangarajan, P.; Register, R. A.; Adamson, D. H.; Fetters, L.; Bras, W.; Naylor, S.; Ryan, A. J. *Macromolecules* **1995**, *28*, 1422.
(14) Rangarajan, P.; Haisch, C. F.; Register, R. A.; Adamson, D. H.; Fetters, L. *Macromolecules* **1997**, *30*, 494.
(15) Okamoto, S.; Yamamoto, K.; Nomura, K.; Hara, S.; Akiba, I.; Sakurai, K.; Koyama, A.; Nomura, M.; Sakurai, S. *J. Macromol. Sci.* **2004**, *43*, 279.
(16) Rangarajan, P.; Register, R. A.; Fetters, L.; Brass, W.; Naylor, S.; Ryan, A. J. *Macromolecules* **1995**, *28*, 4932.
(17) Nojima, S.; Kato, K.; Tamamoto, S.; Ashida, T. *Macromolecules* **1992**, *25*, 2237.
(18) Loo, Y.; Register, R.; Ryan, A.; Dee, G. *Macromolecules* **2001**, *34*, 8968.
(19) Loo, Y.; Register, R.; Ryan, A. *Macromolecules* **2002**, *35*, 2365.
(20) Lorenzo, A. T.; Arnal, M. L.; Müller, A. J.; Boschetti de Fierro, A.; Abetz, V. *Eur. Polym. J.* **2006**, *42*, 516.
(21) Hamley, I. W. *Adv. Polym. Sci.* **1999**, *148*, 113.
(22) Grulke, E. A. In *Polymer Handbook*, 4th ed.; Brandrup, J., Immergut, E. H., Grulke, E. A., Eds.; Wiley & Sons: New York, 1999; VII/675.
(23) Fillon, B.; Wittman, J. C.; Lotz, B.; Thierry, A. *J. Polym. Sci., Part B* **1993**, *31*, 1383.
(24) Lorenzo, A. T.; Arnal, M. L.; Sánchez, J. J.; Müller, A. J. *J. Polym. Sci., Polym. Phys.* **2006**, *44*, 1738.
(25) Müller, A. J.; Hernández, Z. H.; Arnal, M. L.; Sanchez, J. J. *Polym. Bull. (Berlin)* **1997**, *39*, 465.
(26) Müller, A. J.; Arnal, M. L. *Prog. Polym. Sci.* **2005**, *30*, 559.
(27) Boschetti-de-Fierro, A.; Müller, A. J.; Abetz, V. *Macromolecules* **2007**, *40*, 1290.
(28) Bates, F. S.; Schultz, M. F.; Rosedale, J. H. *Macromolecules* **1992**, *25*, 5547.
(29) Ryan, A. J.; Hamley, I. W.; Bras, W.; Bates, F. S. *Macromolecules* **1995**, *28*, 3860.
(30) Schmalz, H.; Müller, A. J.; Abetz, V. *Macromol. Chem. Phys.* **2003**, *204*, 111.
(31) Hech, B.; Strobl, G.; Grasruck, M. *Eur. Phys. J. E* **2003**, *22*, 117.
(32) Müller, A. J.; Balsamo, V.; Arnal, M. L.; Jakob, T.; Schmalz, H.; Abetz, V. *Macromolecules* **2002**, *35*, 3048.
(33) Müller, A. J.; Arnal, M. L.; López-Carrasquero, F. *Macromol. Symp.* **2002**, *183*, 199.
(34) Arnal, M. L.; López-Carrasquero, F.; Laredo, E.; Müller, A. J. *Eur. Polym. J.* **2004**, *40*, 1461.
(35) Balsamo, V.; Paolini, Y.; Ronca, G.; Müller, A. J. *Macromol. Chem. Phys.* **2000**, *201*, 2711.
(36) Müller, A. J.; Lorenzo, A. T.; Arnal, M. L.; Boschetti de Fierro, A.; Abetz, V. *Macromol. Symp.* **2006**, *240*, 114.
(37) Lorenzo, A. T.; Arnal, M. L.; Müller, A. J.; Boschetti de Fierro, A.; Abetz, V. *Macromol. Chem. Phys.* **2006**, *207*, 39.
(38) Wunderlich, B. In *Macromolecular Physics;* Academic Press: New York, 1980; Vol. 3.
(39) Okui, N.; Kawai, T. *Makromol. Chem.* **1972**, *156*, 161.
(40) Balsamo, V.; Urdaneta, N.; Pérez, L.; Carrizales, P.; Abetz, V.; Müller, A. J. *Eur. Polym. J.* **2004**, *40*, 1033.
(41) Alizadeh, A.; Richardson, L.; Xu, J.; McCartney, S.; Marand, H.; Cheung, Y. W. *Macromolecules* **1999**, *32*, 6221.
(42) Crist, B.; Claudio, E. S. *Macromolecules* **1999**, *32*, 8945.
(43) Crist, B.; Williams, D. N. *J. Macromol. Sci., Phys.* **2000**, *B39*, 1.
(44) Mandelkern, L.; Alamo, R. G. Thermodynamic quantities governing melting. In *Physical Properties of Polymers Handbook*; Mark, J. E., Ed.; American Institute of Physics: Woodbury, NY, 1996; p 119.
(45) Avrami, M. *J. Chem. Phys.* **1939**, *7*, 1103.
(46) Avrami, M. *J. Chem. Phys.* **1940**, *8*, 212.
(47) Avrami, M. *J. Chem. Phys.* **1941**, *9*, 177.
(48) Evans, U. R. *Trans. Faraday. Soc.* **1945**, *41*, 365.
(49) Mandelkern, L.; Quinn, F. A.; Flory, P. J. *J. Appl. Phys.* **1954**, *25*, 830.
(50) Piorkowska, E.; Galeski, A.; Haudin, J. M. *Prog. Polym. Sci.* **2006**, *31* 549.
(51) Mandelkern, L. In *Crystallization of Polymers*, 2nd ed.; Cambridge University Press: Cambridge, 2002; Vol. 1.
(52) Mandelkern, L. In *Physical Properties of Polymers*, 3rd ed.; Mark, J. E., Ed.; Cambridge University Press: Cambridge, 2004.
(53) Shultz, J. M. In *Polymer Crystallization*; Oxford University Press: London, 2001.
(54) Takeshita, H.; Ishii, N.; Araki, C.; Miya, M.; Takenaka, K.; Shiomi, T. *J. Polym. Sci., Polym. Phys.* **2004**, *42*, 4199.
(55) Massa, M. V.; Carvalho, J. L.; Dalnoki-Veress, K. *Eur. Phys. J. E* **2003**, *12*, 111.
(56) Massa, M. V.; Dalnoki-Veress, K. *Phys. Rev. Lett.* **2004**, *92*, 255509.
(57) Lambert, W. S.; Phillips, P. J. *Macromolecules* **1994**, *27*, 3537.
(58) Müller, A. J.; Albuerne, J.; Marquez, L.; Raquez, J.-M.; Degée, P.; Dubois, P.; Hobbs, J.; Hamley, I. W. *Faraday Discuss.* **2005**, *128*, 231.
(59) Reiter, G.; Strobl, G. R. In *Progress in Understanding of Polymer Crystallization, Series: Lecture Notes in Physics*; Springer: Heidelberg, Germany, 2007; Vol. 714.
(60) Lauritzen, J. I., Jr.; Hoffman, J. D. *J. Res. Natl. Bur. Stand. Sect. A* **1961**, *64*, 73.
(61) Hoffman, J. D.; Lauritzen, J. I., Jr. *J. Res. Natl. Bur. Stand. Sect. A* **1961**, *65*, 297.
(62) Strobl, G. A Multiphase Model Describing Polymer Crystallization and Melting. In *Progress in Understanding of Polymer Crystallization, Series: Lecture Notes in Physics*; Springer: Heidelberg, Germany, 2007; Vol. 714, Chapter 23.
(63) Hobbs, J. K. A Multiphase Model Describing Polymer Crystallization and Melting. In *Progress in Understanding of Polymer Crystallization, Series: Lecture Notes in Physics*; Springer: Heidelberg, Germany, 2007; Vol. 714, Chapter 23.
(64) Flory, P. J. *Trans. Faraday Soc.* **1955**, *51*, 848.
(65) Boon, J.; Azcue, J. M. *J. Polym. Sci.* **1968**, *6*, 885.

MA070252L